Theoretical Investigation on Intramolecular Friedel-Crafts Alkylation Of 2,2′-Disubstituted 1,3-Indandione Delivering Axially Chiral Biaryls Catalyzed by Chiral Phosphoric Acid

Nan Lu* and Chengxia Miao

College of Chemistry and Material Science, Shandong Agricultural University, Taian 271018, P. R. China.

*Corresponding Author: Nan Lu, College of Chemistry and Material Science, Shandong Agricultural University, Taian 271018, P. R. China.

Abstract:

Our Density Functional Theory (DFT) calculations provide the first theoretical investigation on CPA-catalyzed intramolecular Friedel-Crafts alkylation of 1,3-indandione. The reaction is initiated by bis-coordination of CPA with carbonyl and phenol of indandione. The promotion of CPA lies in H-bridge and steric effect from big silyl substituents confirming less-hindered Re-face more favorable than more-shielded Si-face within central chiral alcohol. Next AlCl3-promoted process contains four steps. The dehydration gives positive carbocation, the rearrangement of which activates another carbonyl. The water reversely splits into hydrogen and hydroxyl to recover phenol. The naphthol is obtained from opening of five-membered ring. The central-to-axial chirality conversion is secured between methyl/phenol substituents and carboxylic moiety of axially chiral biaryls. The positive solvation effect is suggested by decreased absolute and activation energies in solution compared with in gas. These results are supported by Multiwfn analysis on FMO composition of specific TSs, and MBO value of vital bonding, breaking.

Key words: central-to-axial conversion; Friedel-Crafts alkylation; rearrangement; aromatization; chiral phosphoric acid

1.Introduction

The structural core of axially chiral bi(hetero)aryl are identified with potential medicinal applications in pharmaceuticals and as natural products [1–3]. This brings various strategies to handling stereochemistry from drug regulatory agencies. The ability of natural receptors possess differential binding between atropisomers and require new techniques for atropselective synthesis of desired targets. The general approach frequently used in asymmetric synthesis for chiral ligands and catalysts has received much attention such as phosphoramidites, the privileged ligands in asymmetric catalysis [4] and binaphthyl scaffold versatile in C–H functionalization [5]. Therefore the enantioselective synthetic method is attractive eliminating unwanted enantiomer and worthy significant efforts devoted to those chiral scaffolds. Bringmann reported atroposelective synthesis of axially chiral biaryl natural products. Kumarasamy analyzed nonbiaryl and heterobiaryl atropisomers as molecular templates [6]. Metrano achieved peptide-based catalysts through remote desymmetrization and atroposelectivity [7]. To synthesize enantio-enriched atropisomer, the central atropchiral framework is always controlled to construct stereogenic axis from non-chiral substrates using chiral catalyst [8-11]. Mei's atropisomers beyond the C–C axial chirality,

Li's axially chiral indole-based frameworks and Zhang's atropisomers bearing multiple chiral elements [12-14]. Besides these methods, the central-to-axial chirality conversion including creation of stereogenic axis and simultaneous destruction of stereogenic center through aromatization become increasingly popular [15]. Thus it is desirable yet challenging to investigate the potential of carbocation generated in enantioselective desymmetrizing of 1,3-diones. Qin discovered desymmetric enantioselective reduction of cyclic 1,3-diketones catalyzed by recyclable phosphinamide organocatalyst [16]. Yang disclosed enantioselective condensation with hydrazine [17]. Barik reported NHC-catalyzed desymmetrization of N-aryl maleimides leading to atroposelective synthesis of N-aryl succinimides [18]. Ghosh obtained fischer indolization through dynamic kinetic resolution [19]. The sophisticated carbocation is expected to be generated via dehydration, which undergoes energetically favored rearrangement and aromatization proposed by Brotschi's oxadiazole derivatives as dual orexin receptor antagonists giving structure–activity relationship [20]. In this field, the contribution of Liu group is remarkable in a recent breakthrough of chiral phosphoric acid (CPA)-catalyzed intramolecular Friedel-Crafts alkylation arising

from 2,2′-disubstituted 1,3-indandione [21]. They also envisioned chiral alcohol featuring adjacent quaternary stereocenter would be generated catalyzed by Brönsted acid CPA. As we know, CPA was previously utilized in atroposelective synthesis of indole derivatives bearing axial chirality and enantioselective synthesis of 3-arylindole atropisomers via indolization of iminoquinones [22,23]. Although axially chiral biaryls were yielded in excellent yields, many problems still puzzled and there was no report about detailed mechanistic study explaining the central-to-axial chirality conversion. Since CPA was proposed to interact with phenol hydroxyl and carbonyl within substrate [24,25], What's specific process of dual hydrogen-bonding activation modes? Why high stereoselectivity for central chiral alcohols was determined by the first desymmerization/functionalization of substrate? Was the construction of axial chirality influenced via Lewis acid (AlCl3)-promoted carbocation rearrangement? To solve these questions in experiment, an in-depth theoretical study was necessary for this strategy also focusing on the exploration of carbocation's potential.

2. Computational details

The geometry optimizations were performed at the B3LYP/BSI level with the Gaussian 09 package [26,27]. The mixed basis set of LanL2DZ for I and 6-31G(d) for other non-metal atoms [28-32] was denoted as BSI. Different singlet and multiplet states were clarified with B3LYP and ROB3LYP approaches including Becke's three-parameter hybrid functional combined with Lee−Yang−Parr correction for correlation [33,34]. The nature of each structure was verified by performing harmonic vibrational frequency calculations. Intrinsic reaction coordinate (IRC) calculations were examined to confirm the right connections among key transition-states and corresponding reactants and products. Harmonic frequency calculations were carried out at the B3LYP/BSI level to gain zero-point vibrational energy (ZPVE) and thermodynamic corrections at 353 K and 1 atm for each structure in toluene. The solvation-corrected free energies were obtained at the B3LYP/6-311++G(d,p) (LanL2DZ for I) level by using integral equation formalism polarizable continuum model (IEFPCM) in Truhlar's "density" solvation model [35-37] on the B3LYP/BSI-optimized geometries. As an efficient method of obtaining bond and lone pair of a molecule from modern ab initio wave functions, NBO procedure was performed with Natural bond orbital (NBO3.1) to characterize electronic properties and bonding orbital interactions [38,39]. The wave function analysis was provided using Multiwfn_3.7_dev package [40] including research on frontier molecular orbital (FMO) and Mayer bond order (MBO).

3 Discussion

The mechanism was explored for CPA-catalyzed intramolecular Friedel-Crafts alkylation of 2,2′-disubstituted 1,3-indandione **1** affording central chiral tertiary alcohol **2** and AlCl3-promoted carbocation rearrangement/aromatization delivering axially chiral biaryl-2-carboxylic acid 3 (Figure 1). Illustrated by Figure 2, the reaction is initiated by bis-coordination of CPA with carbonyl and phenol motif of **1** (black arrow). With bis-trimethyl silyl substituents of model CPA, the indandione **1** can be positioned in two ways allowing the subsequent intramolecular Friedel-Crafts alkylation to take place from less-hindered Re-face or more-shielded Si-face of carbonyl, leading to desymmetrization and stereoselectivity within tertiary alcohol **2**. The "r" and "s" prefixes are used for stationary points on two parallel paths respectively. Two steps are located for this process that is nucleophilic attack and proton transfer. Then based on the coordination of phenol and hydroxyl of **2** with AlCl3 (red arrow), intermediate **i3** is formed which undergoes dehydration assisted by AlCl3 giving positive C6 adjacent to quaternary chiral center C5 within carbocation **i4**. The rearrangement of **i4** from the dissociation of AlCl3 with water affords **i5**, where another carbonyl residual is activated by AlCl3 (blue arrow). The water molecule reversely splits into hydrogen and hydroxyl group to recover phenol and link to positive C6 in **i5-1**. In next step the hydroxyl is bonded to C7 yielding carboxyl group of **i5-2**. Finally the conjugated naphthol structure is obtained from opening of five-membered ring with concerted double bond formation in axially chiral biaryls **3**, in which the excellent central-to-axial chirality conversion is secured between methyl/phenol substituents and carboxylic moiety.

The schematic structures of optimized TSs in Figure 2 were listed by Figure 3. The activation energy was shown in Table 1 for all steps. Supplementary Table S1, Table S2 provided the relative energies of all stationary points. According to experiment, the Gibbs free energies in toluene solution phase are discussed here [21]. However, in order to save computing resources, methyl was used to replace phenyl group of catalyst CPA in experiment. This makes an absolutely accurate prediction of stereoselectivities unavailable for this study.
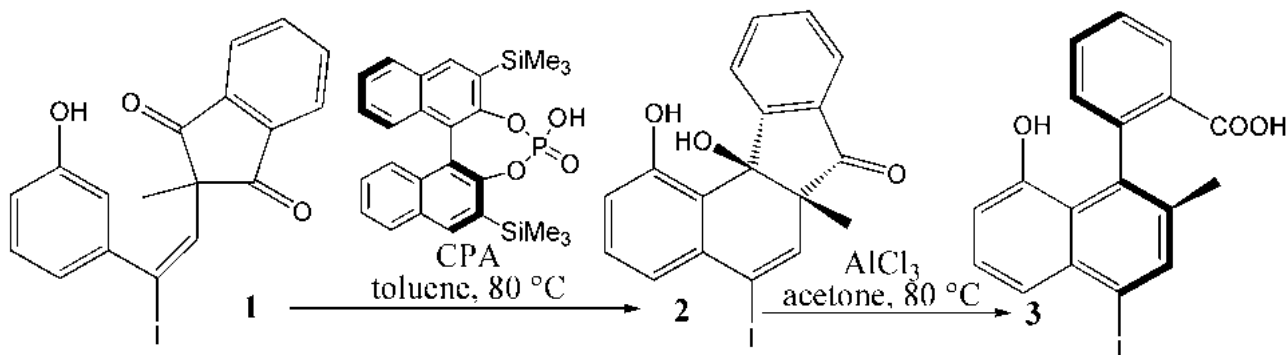
Figure 1: CPA-catalyzed intramolecular Friedel-Crafts alkylation of 2,2′-disubstituted 1,3-indandione **1** affording central chiral tertiary alcohol **2** and AlCl3-promoted carbocation rearrangement/aromatization delivering axially chiral biaryl-2-carboxylic acid **3**.

Species	ΔG_{gas}	$\Delta G_{sol(toluene)}$
1	0.00	0.00
2	-5.60	-3.78
3	-25.79	-23.86
1+CPA	0.00	0.00
r-i1	-412.88	-412.13
r-tsi12-0	-388.65	-387.88
r-i1-1	-396.98	-395.01
r-tsi12-1	-360.86	-359.52
r-i2	-413.67	-419.65
s-i1	-414.89	-413.46
s-tsi12-0	-384.26	-381.86
s-i1-1	-396.78	-395.20
s-tsi12-1	-360.88	-359.63
s-i2	-406.68	-408.69
1+AlCl3	0.00	0.00
i3	-101.87	-101.47
tsi34	-94.97	-96.59
i4	-106.58	-108.16
i5	-98.09	-99.90
tsi56-0	-80.42	-82.43
i5-1	-111.56	-112.99
tsi56-1	-82.98	-85.11
i5-2	-87.95	-93.40
tsi56-2	-86.29	-90.31
i6	-134.65	-134.48

Table S1. Calculated relative energies (all in kcal mol^{-1}, relative to isolated species) for the ZPE-corrected Gibbs free energies (ΔG_{gas}), Gibbs free energies for all species in solution phase (ΔG_{sol}) at 353 K by B3LYP/6-311++G(d,p)//B3LYP/6-31G(d) method and difference between absolute energy.

TS	$\Delta G^{\neq}_{gas}$	$\Delta G^{\neq}_{sol}$
r-tsi12-0 (294i)	24.2	24.2
r-tsi12-1 (1393i)	36.1	35.5
s-tsi12-0 (282i)	30.6	31.6
s-tsi12-1 (1398i)	35.9	35.6
tsi34 (167i)	6.9	4.9
tsi56-0 (508i)	17.7	17.4
tsi56-1 (390i)	28.6	27.9
tsi56-2 (234i)	1.7	3.1

Table S2. The activation energy (local barrier) (in kcal mol^{-1}) of all reactions in the gas, solution phase calculated with B3LYP/6-311++G(d,p)//B3LYP/6-31G(d) method.

	C1⋯C6	O3⋯H1	O2⋯H2	
r-tsi12-0	0.52	0.23	0.46	
	C1⋯H3	H3⋯O2	O2⋯H2	H2⋯O4
r-tsi12-1	0.50	0.29	0.23	0.49
	O1⋯H1	H1⋯O2	C6⋯O2	
ts-i34	0.46	0.39	0.25	
	O1⋯H1	H1⋯O2	C6⋯O2	
tsi56-0	0.27	0.49	0.39	
	C6⋯O2	O2⋯C7		
tsi56-1	0.37	0.54		
	C5⋯C7	C5⋯C6		
tsi56-2	0.62	1.25		

Table S3. Mayer bond order (MBO) of typical TSs
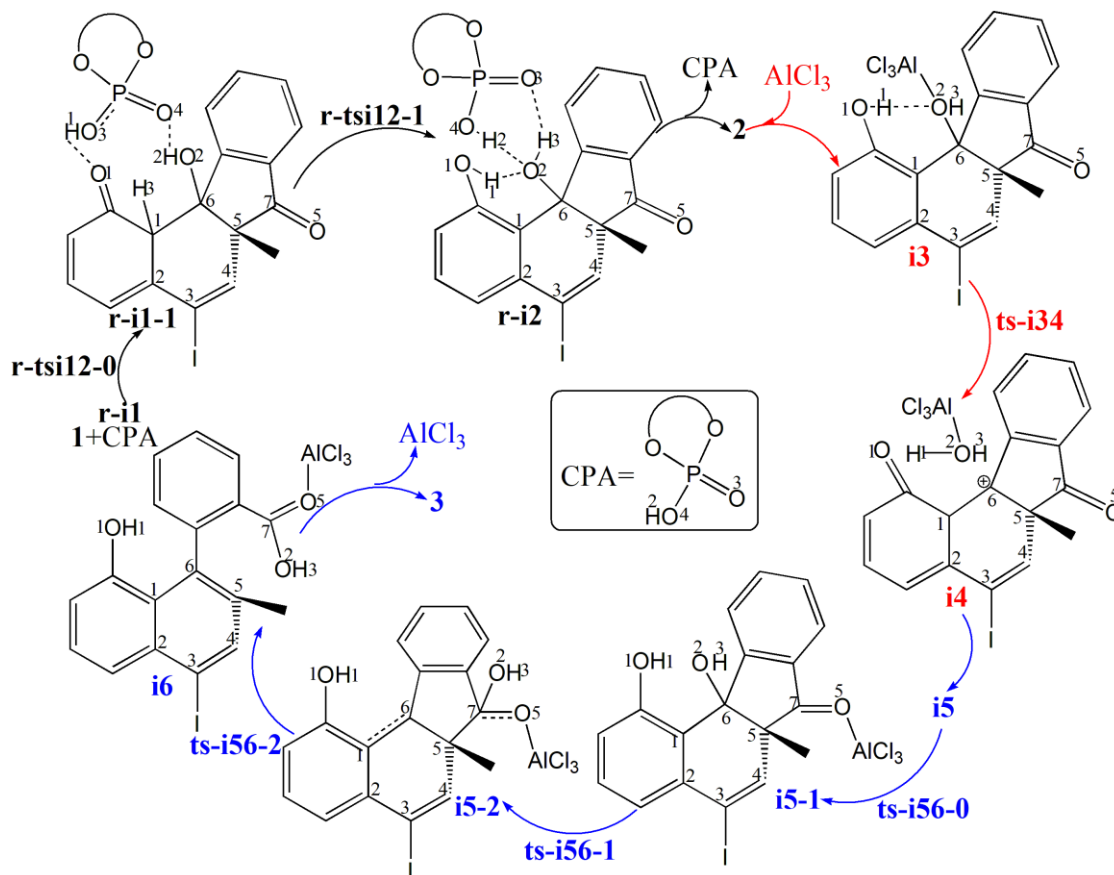
Figure 2: Proposed reaction mechanism of CPA-catalyzed intramolecular Friedel-Crafts alkylation of **1** affording **2** and AlCl3-promoted carbocation rearrangement/aromatization delivering **3**. TS is named according to the two intermediates it connects.

TS	$\Delta G^{\neq}_{gas}$	$\Delta G^{\neq}_{sol}$
r-tsi12-0	24.2	24.2
r-tsi12-1	36.1	35.5
s-tsi12-0	30.6	31.6
s-tsi12-1	35.9	35.6
tsi34	6.9	4.9
tsi56-0	17.7	17.4
tsi56-1	28.6	27.9
tsi56-2	1.7	3.1

Table 1: The activation energy (in kcal mol^{-1}) of all reactions in gas and solvent

(a)
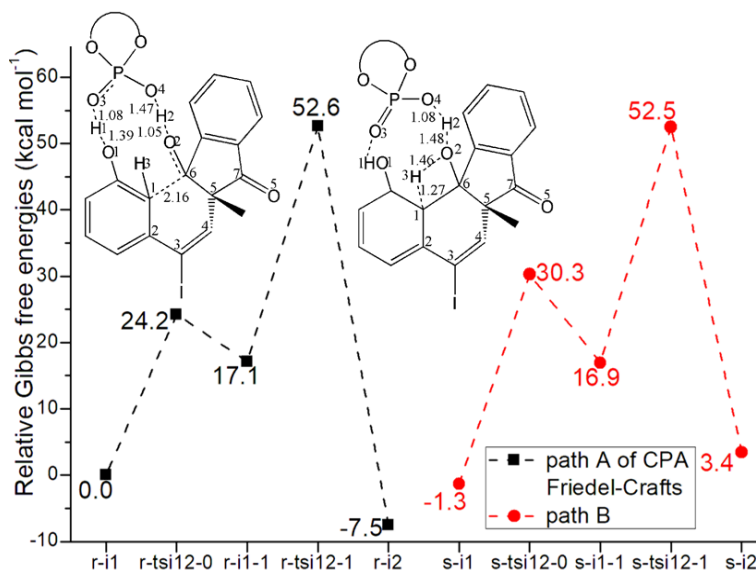
(b)
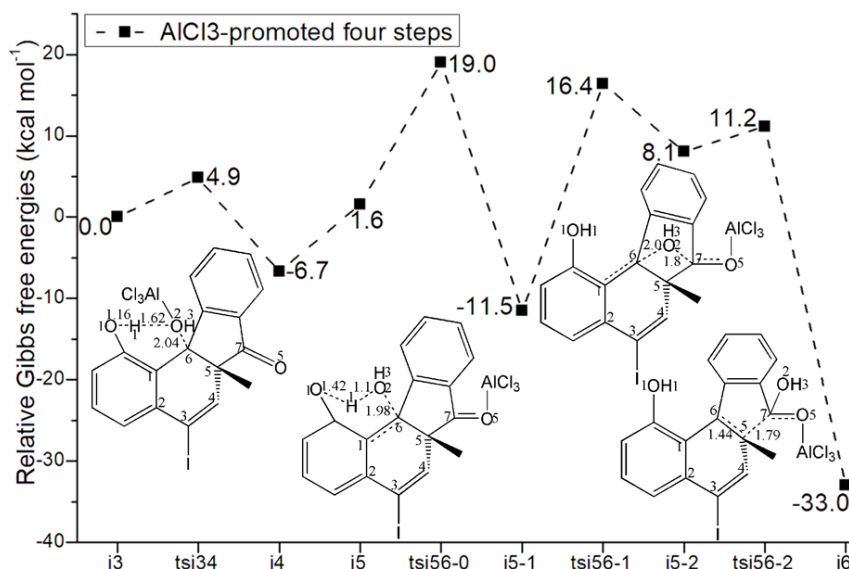
Figure 3: Relative Gibbs free energy profile in solvent phase starting from complex (a) **r-i1** (b) **i3** (Bond lengths of optimized TSs in Å).

3.1 CPA-catalyzed intramolecular Friedel-Crafts alkylation

Two steps are located for the first phase of CPA-catalyzed intramolecular Friedel-Crafts alkylation. Owing to the same process, "r" stationary points from less-hindered Re-face will be discussed in detail denoted as path A (black dash line of Figure 3a). The initial complex **r-i1** is stabilized by bis-coordination of CPA with carbonyl and phenol motif of **1** forming H bond depending on P-O4H2 and P=O3. The intramolecular nucleophilic addition proceeds via **r-tsi12-0** in step 1 with the activation energy of 24.2 kcal mol^{-1} relative to the starting point **r-i1** endothermic by 17.1 kcal mol^{-1} producing **r-i1-1**. The transition vector contains two parts in concerted modes that is dual proton transfer of H1 from O1 to O3 and H2 from O4 to O2 followed by approaching of negative C1 to positive C6 (1.39, 1.08, 1.47, 1.05, 2.16 Å) (Figure S1a). Obviously with formal C1-C6 single bond, the new six-membered ring in **r-i1-1** is reactive to initiate next step.

Then mediated by CPA, the proton transfer occurs via **r-tsi12-1** as step 2 with activation energy of 35.5 kcal mol^{-1} exothermic by -7.5 kcal mol^{-1}

giving intermediate **r-i2**. The transition vector includes proton H3 on sp3 hybrid C1 moving to O2 along with cooperated retuning of H2 from O2 to O4 (1.27, 1.46, 1.48, 1.08 Å) (Figure S1b). In stable **r-i2**, O2H3 not only forms bis-coordination with CPA via two H bonds but makes inter O1-H1···O2 available. In addition, C1 recovers sp2 hybrid of phenol after kicking off H3. Clearly during two steps of the first phase, CPA constantly functions as LA providing H-bridge driving force. When Friedel-Crafts alkylation is completed, the central chiral tertiary alcohol **2** is obtained after removal of CPA.

3.2   AlCl₃-promoted   dehydration/carbocation rearrangement/carboxyl formation/aromatization

Four steps are located in next phase promoted by AlCl₃, which plays role of BA accepting lone pair of hydroxyl or carbonyl. The initial intermediate **i3** is formed with Al-O2H3 coordination taken as new starting point of the four steps (black dash line of Figure 3b). Assisted by AlCl₃, the dehydration undergoes in step 3 via **ts-i34** with activation energy of 4.9 kcal mol^{-1} affording **i4** exothermic by -6.7 kcal mol^{-1}.

According to the transition vector, O2H3 and H1 donated by phenol O1 assembles water molecule, which is ruptured from C6 afterwards that is remarkable O1···H1···O2 and C6···O2 cleavage (1.16, 1.62, 2.04 Å) (Figure S1c). Taken away of water by AlCl₃ affords positive C6 adjacent to quaternary chiral center C5 within carbocation **i4**. Subsequently, the rearrangement of **i4** generates reactive **i5** with increased relative energy. This is achieved through dissociation of AlCl₃ with water and turns to activate another carbonyl residual C7=O5 forming Al-O5 single bond. In step 4, the water molecule H1O2H3 reversely splits into hydrogen H1 and hydroxyl O2H3 to recover phenol and link to positive C6. An intermediate **i5-1** is delivered via **tsi56-0** with activation energy of 17.4 kcal mol⁻¹ exothermic by -11.5 kcal mol⁻¹ . The transition vector corresponds to O2···H1···O1 and O2···C6 linkage (1.1, 1.42, 1.98 Å) just opposite to the case of **ts-i34** (Figure S1d). Although characterized by similar structure with **i3**, **i5-1** becomes more stable with lower energy indicating this worthy transformation. Next, hydroxyl O2H3 moves from C6 to C7 via **tsi56-1** in step 5 with activation energy of 27.9 kcal mol⁻¹ endothermic by 8.1 kcal mol⁻¹ yielding carboxyl group of **i5-2**. The transition vector reveals breaking of O2···C6 and bonding of O2-C7 (2.0,

1.8 Å) (Figure S1e). **i5-2** is quite reactive ready for the final step. Consequently, the opening of five-membered ring proceeds via **tsi56-2** in step 6 with small activation energy of 3.1 kcal mol⁻¹ enormously exothermic by -33.0 kcal mol⁻¹. In resultant **i6**, the conjugated naphthol structure is obtained via aromatization that is simultaneous new C5-C6 double bond formation. The detailed atomic motion is illustrated according to the transition vector about dissociation of C5-C7 and shortening of C5-C6 bond from single to double (1.79, 1.44 Å) (Figure S1f). Once AlCl₃ is left, axially chiral biaryls **3** is achieved denoting central-to-axial chirality conversion between methyl/phenol substituents and carboxylic moiety. Comparatively, proton transfer mediated by CPA of step 2 is determined to be rate-limiting for the whole process. To highlight the idea of feasibility for changes in electron density and not molecular orbital interactions are responsible of the reactivity of organic molecules, quantum chemical tool Multiwfn was applied to analyze of electron density such as MBO results of bonding atoms and contribution of atomic orbital to HOMO of typical TSs (Table S3, Figure S2). These results all confirm the above analysis.

(a)

(b)

(c)

(d)
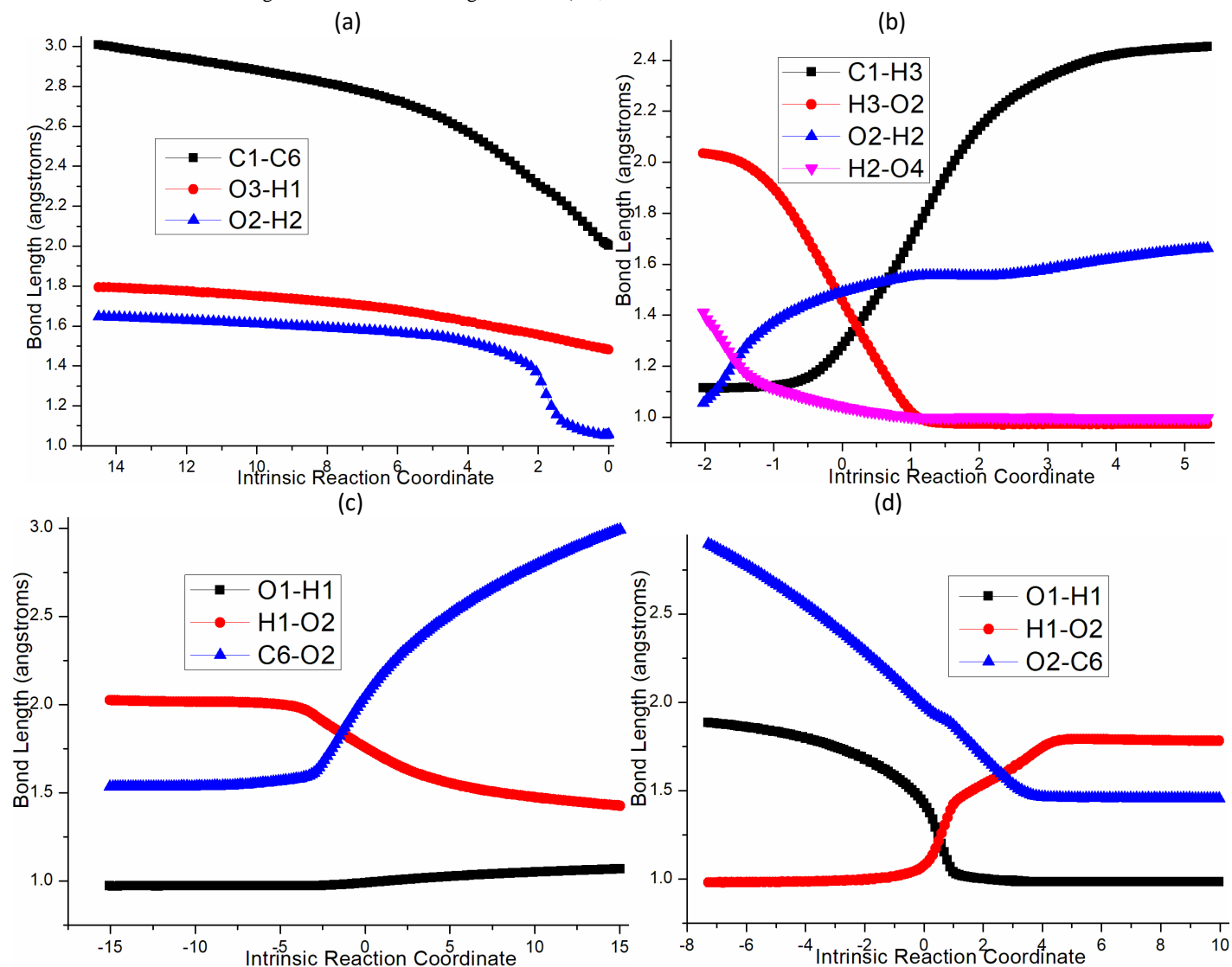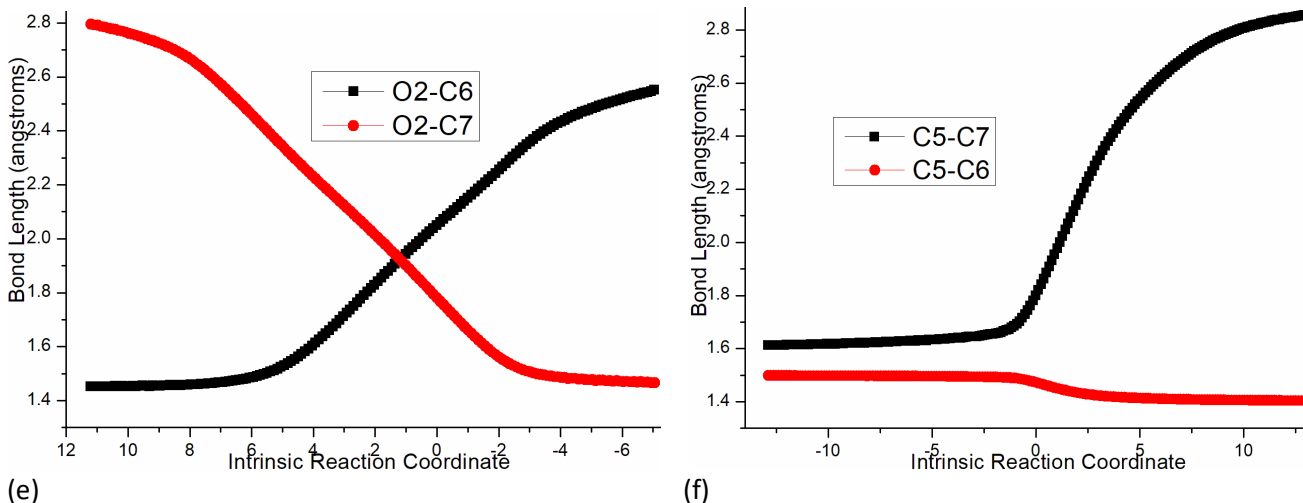
Figure S1. Evolution of bond lengths along the IRC for (a) **r-tsi12-0** (b) **r-tsi12-1** (c) **ts-i34** (d) **tsi56-0** (e) **tsi56-1** (f) **tsi56-2** at B3LYP/6-311++G(d,p) level.
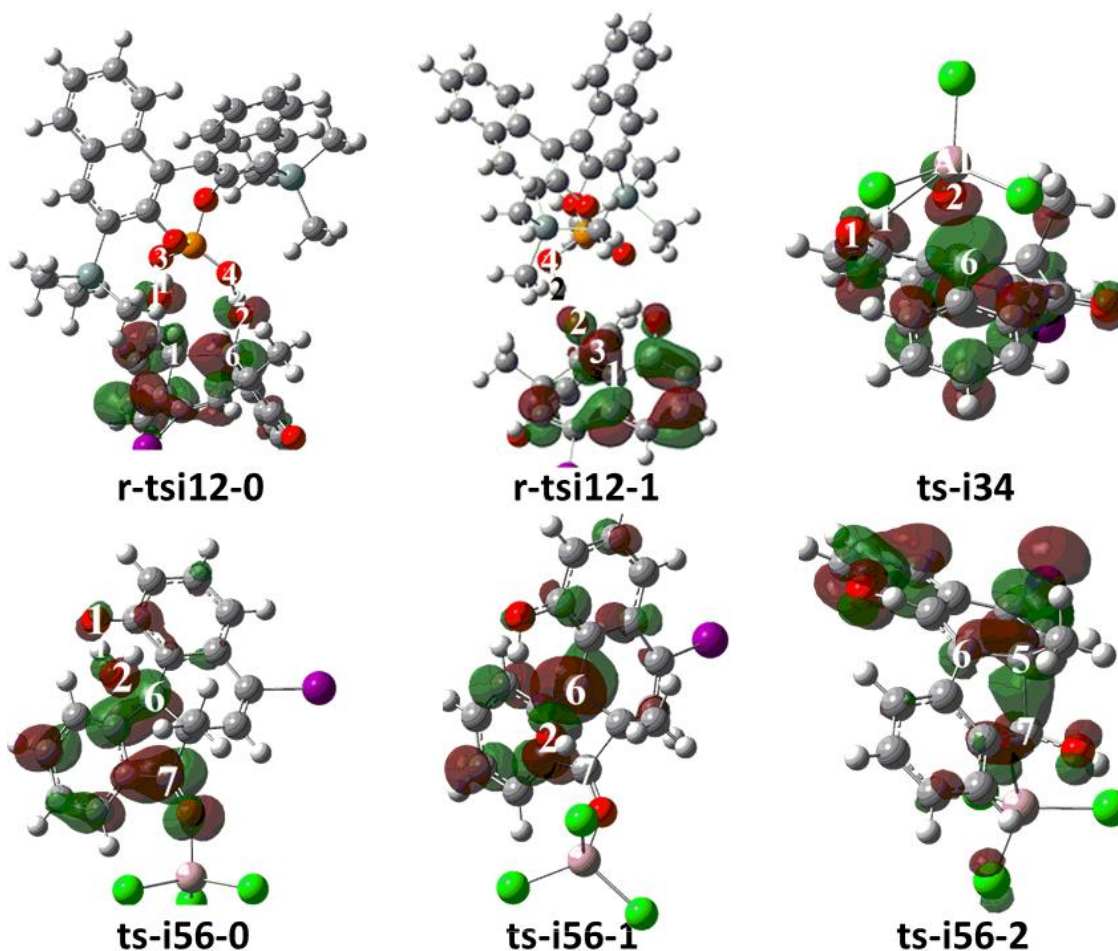
Figure S2. Highest Occupied Molecular Orbital (HOMO) of typical TSs. Different colors are used to identify the phase of the wave functions.

3.3 Desymmetrization and stereoselectivity within central chiral alcohol

To investigate the promotion of CPA, the desymmetrization and stereoselectivity within tertiary alcohol are also explored via comparison between parallel path B from more-shielded Si-face of the previous two steps (red dash line of Figure 3a). The complex between **1**, **2** and BF$_3$·OEt$_2$ is denoted as **i1**. The nucleophilic addition proceeds via **s-tsi12-0** in step 1 with activation energy of 31.6 kcal mol^{-1} relative to the starting point **s-i1** endothermic by 16.9 kcal mol^{-1} producing **s-i1-1**. The proton transfer occurs via **s-tsi12-1** as step 2 with activation energy of 35.6 kcal mol^{-1} endothermic by 3.4 kcal mol^{-1} giving **s-i2**. Evidently, the significant difference lies in barrier of path A from less-hindered Re-face lower than that of path B from more-shielded Si-face (24.2 vs 31.6 kcal

mol^{-1}). What's more, the relative energy of Friedel-Crafts product **r-i2** is also lower than that of **s-i2** (-7.5 vs 3.4 kcal mol^{-1}). Hence, the steric effect arrtibuted by bis-trimethyl silyl substituents of CPA differentiates Friedel-Crafts alkylation from less-hindered Re-face or more-shielded Si-face of carbonyl confirming the former advantageous both from kinetics and thermodynamics leading to desymmetrization and stereoselectivity within tertiary alcohol [21].

4 Conclusions

Our DFT calculations provide the first theoretical investigation on CPA-catalyzed intramolecular Friedel-Crafts alkylation of 2,2′-disubstituted 1,3-indandione. The reaction is initiated by bis-coordination of CPA with carbonyl and phenol of indandione via two steps of nucleophilic attack and proton transfer with the latter determined to be rate-limiting. The promotion of CPA not only lies in H-bridge driving force but steric effect attributed by big silyl substituents confirming less-hindered Re-face more favorable than more-shielded Si-face both from kinetics and thermodynamics leading to desymmetrization and stereoselectivity within central chiral alcohol. Next as BA accepting lone pair of hydroxyl or carbonyl, AlCl$_3$-promoted process contains four steps. The dehydration undergoes giving positive carbocation. The rearrangement of carbocation arises from dissociation of water with AlCl$_3$, which activates another carbonyl. The water molecule reversely splits into hydrogen and hydroxyl to recover phenol. Then hydroxyl turns from positive carbon to carbonyl carbon yielding carboxyl group. Finally the conjugated naphthol is obtained from opening of five-membered ring with concerted double bond formation. The central-to-axial chirality conversion is secured between methyl/phenol substituents and carboxylic moiety of axially chiral biaryls. The positive solvation effect is suggested by decreased absolute and activation energies in toluene solution compared with in gas. These results are supported by Multiwfn analysis on FMO composition of specific TSs, and MBO value of vital bonding, breaking.

Electronic Supplementary Material

Supplementary data available: [Computation information and cartesian coordinates of stationary points; Calculated relative energies for the ZPE-corrected Gibbs free energies (ΔG_{gas}), and Gibbs free energies (ΔG_{sol}) for all species in solution phase at 353 K.]

References

1. Clayden, J.; Moran, W.; Edwards, P.; LaPlante, S. (2009). The Challenge of Atropisomerism in Drug Discovery. *Angew Chem Int Ed*, 48, 6398–6401.
2. Smyth, J. E.; Butler, N. M.; Keller, P. A. (2015). A twist of nature – the significance of atropisomers in biological systems. Nat Prod Rep, 32, 1562–1583.
3. Lassaletta JM. (2019). Atropisomerism and Axial Chirality. London, England: World Scientific Europe.
4. Teichert, J.; Feringa, B. (2010). Phosphoramidites: Privileged Ligands in Asymmetric Catalysis. *Angew Chem Int Ed*, 49, 2486–2528.
5. Yue, Q.; Liu, B.; Liao, G.; Shi, B. F. (2022). Binaphthyl Scaffold: A Class of Versatile Structure in Asymmetric C–H Functionalization. *ACS Catal*, 12, 9359–9396.
6. Kumarasamy, E.; Raghunathan, R.; Sibi, M. P.; Sivaguru, J. (2015). Nonbiaryl and Heterobiaryl Atropisomers: Molecular Templates with Promise for Atropselective Chemical Transformations. *Chem Rev*, 115, 11239–11300.
7. Metrano, A. J.; Miller, S. J. (2019). Peptide-Based Catalysts Reach the Outer Sphere through Remote Desymmetrization and Atroposelectivity. *Acc Chem Res*, 52, 199–215.
8. Bringmann, G.; Gulder, T. Gulder, T. A. M.; Breuning, M. (2011). Atroposelective Total Synthesis of Axially Chiral Biaryl Natural Products. *Chem Rev*, 111, 563–639.
9. Wang, Y. B.; Tan, B. (2018). Construction of Axially Chiral Compounds via Asymmetric Organocatalysis. *Acc Chem Res*, 51, 534–547.
10. Zilate, B.; Castrogiovanni, A.; Sparr, C. (2018). Catalyst-Controlled Stereoselective Synthesis of Atropisomers. *ACS Catal*, 8, 2981–2988.
11. Cheng, J. K.; Xiang, S. H.; Li, S.; Ye, L.; Tan, B. (2021). Recent Advances in Catalytic Asymmetric Construction of Atropisomers. *Chem Rev*, 121, 4805–4902.
12. Mei, G. J.; Koay, W. L.; Guan, C. Y.; Lu, Y. (2022). Atropisomers beyond the C–C axial chirality: Advances in catalytic asymmetric synthesis. *Chem*, 8, 1855–1893.
13. Li, T. Z.; Liu, S. J.; Tan, W.; Shi, F. (2020). Catalytic Asymmetric Construction of Axially Chiral Indole-Based Frameworks: An Emerging Area. *Chem Eur J*, 26, 15779–15792.
14. Zhang, H. H.; Li, T. Z.; Liu, S. J.; Shi, F. (2024). Catalytic Asymmetric Synthesis of Atropisomers Bearing Multiple Chiral Elements: An Emerging Field. *Angew Chem Int Ed*, 63, e202311053.
15. Lemaitre, C.; Perulli, S.; Quinonero, O.; Bressy, C.; Rodriguez, J. et al. (2023). Enantioselective Synthesis of Atropisomers by Oxidative Aromatization with Central-to-Axial Conversion of Chirality. *Molecules*, 28, 3142.
16. Qin, X. L.; Li, A.; Han, F. S. (2021). Desymmetric Enantioselective Reduction of Cyclic 1,3-Diketones Catalyzed by a Recyclable P-Chiral Phosphinamide Organocatalyst. *J Am Chem Soc*, 143, 2994–3002.
17. Yang, B.; Dai, J.; Luo, Y.; Lau, K. K.; Lan, Y. et al. (2021). Desymmetrization of 1,3-Diones by Catalytic Enantioselective Condensation with Hydrazine. *J Am Chem Soc*, 143, 4179–4186.
18. Barik, S.; Shee, S.; Das, S.; Gonnade, R. G.; Jindal, G. et al. (2021). NHC-Catalyzed Desymmetrization of N-Aryl Maleimides Leading to the Atroposelective Synthesis of N-Aryl Succinimides. *Angew Chem Int Ed*, 60, 12264–12268.
19. Ghosh, B.; Balhara, R.; Jindal, G.; Mukherjee, S. (2021). Catalytic Enantioselective Desymmetrizing Fischer Indolization through Dynamic Kinetic Resolution. *Angew Chem Int Ed*, 60, 9086–9092.
20. Brotschi, C.; Roch, C.; Gatfield, J.; Treiber, A.; Williams, J. et al. (2019). Oxadiazole Derivatives as Dual Orexin Receptor Antagonists: Synthesis, Structure–Activity Relationships, and Sleep-Promoting Properties in Rats. *ChemMedChem*, 14, 1257–1270.
21. Liu, Q.; Liu, S. D.; Cheng, L.; Liu, L. (2024). An Unprecedented Synthesis of Axially Chiral Biaryls by Rearrangement and Aromatization of Carbocations with Central-to-Axial Conversion of Chirality Sci. China Chem. DOI: 10.1007/s11426-024-2035-7.

22. Zhang, H. H.; Shi F. (2022). Organocatalytic Atroposelective Synthesis of Indole Derivatives Bearing Axial Chirality: Strategies and Applications. *Acc Chem Res*, 55, 2562–2580.

23. Liu, Y. W.; Chen, Y. H.; Cheng, J. K.; Xiang, S. H.; Tan B. (2023). Enantioselective synthesis of 3-arylindole atropisomers via organocatalytic indolization of iminoquinones. *Chem Synth,* 3, 11.

24. Lin, X.; Wang, L.; Han, Z.; Chen, Z. (2021). Chiral Spirocyclic Phosphoric Acids and Their Growing Applications. *Chin J Chem*, 39: 802–824.

25. Jiménez, E. I. (2023). An update on chiral phosphoric acid organocatalyzed stereoselective reactions. *Org Biomol Chem*, 21: 3477–3502.

26. Frisch, M. J.; Trucks, G. W.; Schlegel, H. B. et al. (2010). Gaussian 09 (Revision B.01), Gaussian, Inc., Wallingford, CT.

27. Hay, P. J.; Wadt, W. R. (1985). Ab initio effective core potentials for molecular calculations-potentials for the transition-metal atoms Sc to Hg. *J. Chem. Phys*. 82, 270-283.

28. Lv, H.; Han, F.; Wang, N.; Lu, N.; Song, Z. et al. (2022). Ionic Liquid Catalyzed C-C Bond Formation for the Synthesis of Polysubstituted Olefins. *Eur. J. Org. Chem*. e202201222.

29. Zhuang, H.; Lu, N.; Ji, N.; Han, F.; Miao, C. (2021). Bu4NHSO4-Catalyzed Direct N-Allylation of Pyrazole and its Derivatives with Allylic Alcohols in Water: A Metal-free, Recyclable and Sustainable System. *Advanced Synthesis & Catalysis*, 363, 5461-5472.

30. Lu, N.; Lan, X.; Miao, C.; Qian, P. (2020). Theoretical investigation on transformation of Cr(II) to Cr(V) complexes bearing tetra-NHC and group transfer reactivity. *Int. J. Quantum Chem*. 120, e26340.

31. Lu, N.; Liang, H.; Qian, P.; Lan, X.; Miao, C. (2020). Theoretical investigation on the mechanism and enantioselectivity of organocatalytic asymmetric Povarov reactions of anilines and aldehydes. *Int. J. Quantum Chem*. 120, e26574.

32. Lu, N.; Wang, Y. (2023). Alloy and Media Effects on the Ethanol Partial Oxidation Catalyzed by Bimetallic Pt6M (M= Co, Ni, Cu, Zn, Ru, Rh, Pd, Sn, Re, Ir, and Pt). Computational and Theoretical Chemistry, 1228, 114252.

33. Catellani, M.; Mealli, C.; Motti, E.; Paoli, P.; Perez-Carrenˇo, E. et al. (2002). Palladium-Arene Interactions in Catalytic Intermediates: An Experimental and Theoretical Investigation of the Soft Rearrangement between η1 and η2 Coordination Modes. *J. AM. CHEM*. SOC, 124, 4336-4346.

34. Marenich, A. V.; Cramer, C. J.; Truhlar, D. G. (2009). Universal Solvation Model Based on Solute Electron Density and on a Continuum Model of the Solvent Defined by the Bulk Dielectric Constant and Atomic Surface Tensions. *J. Phys. Chem*. B, 113, 6378–6396.

35. Tapia, O. (1992). Solvent effect theories: Quantum and classical formalisms and their applications in chemistry and biochemistry. *J. Math. Chem*. 10, 139-181.

36. Tomasi, J.; Persico, M. (1994). Molecular Interactions in Solution: An Overview of Methods Based on Continuous Distributions of the Solvent. Chem. *Rev*. 94, 2027-2094.

37. Tomasi, J.; Mennucci, B.; Cammi, R. (2005). Quantum Mechanical Continuum Solvation Models. Chem. Rev. 2005, 105, 2999-3093.

38. Reed, A. E.; Weinstock, R. B.; Weinhold, F. (1985). Natural population analysis. *J. Chem. Phys*. 83, 735-746.

39. Reed, A. E.; Curtiss, L. A.; Weinhold, F. (1988). Intermolecular interactions from a natural bond orbital donor-acceptor view point. *Chem. Rev*. 88, 899-926.

40. Lu, T.; Chen, F. (2012). Multiwfn: A multifunctional wavefunction analyzer. *J. Comput. Chem*. 33, 580-592.

To Submit Your Article Click Here: **Submit Manuscript**

Ready to submit your research? Choose Auctores and benefit from:

- ➢ fast, convenient online submission
- ➢ rigorous peer review by experienced research in your field
- ➢ rapid publication on acceptance
- ➢ authors retain copyrights
- ➢ unique DOI for all articles
- ➢ immediate, unrestricted online access

At Auctores, research is always in progress.

Learn more https://auctoresonline.org/journals/international-journal-of-clinical-case-reports-and-reviews

Software: GAUSSIAN09

Level of Theory: B3LYP

Basis Set: BSI

Geometry [Cartesian coordinates]:

Optimized Cartesian coordinates for **s-tsi12-0**

Center Number	Atomic Number	Atomic Type	X	Y	Z
1	15	0	-1.160611	0.108330	-0.264152
2	8	0	-1.862639	-1.100013	0.548259
3	8	0	-2.394209	1.003030	-0.810658
4	8	0	-0.393976	0.842286	0.875216
5	8	0	-0.335243	-0.303868	-1.452376
6	6	0	-5.201148	-3.022386	-1.080581
7	6	0	-5.310830	-1.654632	-0.672408
8	6	0	-6.528157	-0.971056	-0.945890
9	6	0	-7.582321	-1.614384	-1.557090
10	6	0	-7.483370	-2.977019	-1.925464
11	6	0	-6.313165	-3.661740	-1.692987
12	6	0	-3.977086	-3.711530	-0.880570
13	6	0	-2.847390	-3.101230	-0.363712
14	6	0	-2.993245	-1.738422	0.014482
15	6	0	-4.180532	-1.025456	-0.041659
16	6	0	-5.242114	0.688978	1.528037
17	6	0	-5.369941	2.055349	1.935018
18	6	0	-6.324755	2.403351	2.929036
19	6	0	-7.107131	1.442064	3.525432
20	6	0	-6.957746	0.085365	3.151083
21	6	0	-6.053757	-0.281894	2.178340
22	6	0	-4.274803	0.355602	0.517126
23	6	0	-3.419171	1.357460	0.083494
24	6	0	-3.533558	2.728950	0.436453
25	6	0	-4.532596	3.036292	1.345216
26	1	0	1.160707	-0.718248	-1.173628
27	1	0	-6.619520	0.075524	-0.680231
28	1	0	-8.498129	-1.066943	-1.763182
29	1	0	-8.325325	-3.472972	-2.400415
30	1	0	-6.214103	-4.704231	-1.986365
31	1	0	-3.941354	-4.758087	-1.173467
32	1	0	-6.414430	3.447894	3.218073
33	1	0	-7.828850	1.717235	4.289523
34	1	0	-7.558683	-0.676416	3.640383
35	1	0	-5.945372	-1.326957	1.912912
36	1	0	-4.686492	4.068548	1.652088
37	14	0	-2.458652	4.163574	-0.231778

38	14	0	-1.224844	-4.099811	-0.227939
39	6	0	-3.633193	5.632136	-0.498574
40	1	0	-4.116758	5.964495	0.427340
41	1	0	-3.072861	6.488199	-0.895322
42	1	0	-4.423679	5.391090	-1.219184
43	6	0	-1.164303	4.636408	1.064818
44	1	0	-1.616380	4.790854	2.051619
45	1	0	-0.394974	3.863226	1.155488
46	1	0	-0.663079	5.569774	0.777146
47	6	0	-1.612088	3.777101	-1.877935
48	1	0	-0.725086	3.152596	-1.733342
49	1	0	-2.279682	3.266743	-2.579983
50	1	0	-1.284768	4.715666	-2.344209
51	6	0	-0.239046	-3.892099	-1.830567
52	1	0	-0.030788	-2.836916	-2.033050
53	1	0	0.718092	-4.425938	-1.771308
54	1	0	-0.793400	-4.294292	-2.687131
55	6	0	-0.182405	-3.603822	1.270314
56	1	0	0.347893	-2.660731	1.109825
57	1	0	-0.794615	-3.490959	2.172065
58	1	0	0.566934	-4.380334	1.471350
59	6	0	-1.700333	-5.927298	-0.033691
60	1	0	-2.245659	-6.321463	-0.899205
61	1	0	-0.791151	-6.531981	0.075461
62	1	0	-2.316979	-6.096889	0.856951
63	6	0	3.467723	3.336867	-0.231472
64	6	0	4.824630	3.267055	-0.038773
65	6	0	5.461458	2.082058	0.429563
66	6	0	4.698876	0.968605	0.691284
67	6	0	3.280591	0.969119	0.440983
68	6	0	2.625418	2.211955	0.065337
69	8	0	1.357789	2.322744	-0.029034
70	6	0	5.264957	-0.346879	1.024603
71	6	0	5.103980	-1.374531	0.189207
72	6	0	5.367884	-0.339465	-2.134114
73	6	0	4.481228	0.580440	-2.881977
74	6	0	3.164027	0.491776	-2.401889
75	6	0	3.122975	-0.413386	-1.232332
76	6	0	4.800287	1.376690	-3.981665
77	6	0	3.770232	2.080957	-4.603357
78	6	0	2.447258	1.967574	-4.142911
79	6	0	2.121880	1.172626	-3.043292
80	8	0	2.057516	-1.109239	-0.893893
81	8	0	6.562651	-0.491641	-2.283058
82	53	0	6.316447	-0.586886	2.885206
83	1	0	2.983308	4.251341	-0.558267
84	1	0	5.439250	4.140269	-0.244568
85	1	0	6.537939	2.057363	0.562492
86	1	0	2.680306	0.252313	0.990208
87	1	0	0.423682	1.440376	0.515493
88	1	0	5.494285	-2.360996	0.416111
89	1	0	5.824265	1.420786	-4.340199
90	1	0	3.985009	2.709945	-5.462721
91	1	0	1.656974	2.507159	-4.657192
92	1	0	1.095427	1.080187	-2.706217
93	6	0	4.464534	-1.180466	-1.175148
94	6	0	4.259909	-2.564643	-1.845106
95	1	0	5.232993	-3.055131	-1.944973
96	1	0	3.598635	-3.183506	-1.233073
97	1	0	3.816338	-2.467901	-2.840648

Optimized Cartesian coordinates for **s-tsi12-1**

Center Number	Atomic Number	Atomic Type	Coordinates (Angstroms)		
			X	Y	Z

1	15	0	5.612742	1.224429	-0.390145
2	8	0	5.117948	2.525854	0.454637
3	8	0	4.413480	0.150388	-0.190724
4	8	0	5.907048	1.637899	-1.791689
5	8	0	6.777399	0.511157	0.383015
6	6	0	3.725134	1.958318	4.356353
7	6	0	2.965818	1.440905	3.259144
8	6	0	1.835339	0.628750	3.551503
9	6	0	1.467050	0.366286	4.853317
10	6	0	2.201394	0.905760	5.935718
11	6	0	3.308654	1.683764	5.687017
12	6	0	4.881772	2.737814	4.093000
13	6	0	5.369757	2.947830	2.815132
14	6	0	4.618110	2.368729	1.754286
15	6	0	3.399827	1.727923	1.917162
16	6	0	1.216674	1.836141	0.599028
17	6	0	0.418141	1.353223	-0.486264
18	6	0	-0.920340	1.809099	-0.628874
19	6	0	-1.451606	2.729379	0.244962
20	6	0	-0.653430	3.236615	1.297207
21	6	0	0.642622	2.801891	1.471767
22	6	0	2.566853	1.354610	0.736837
23	6	0	3.073506	0.551833	-0.272370
24	6	0	2.305516	0.032370	-1.352051
25	6	0	0.983313	0.435724	-1.409705
26	1	0	7.685604	0.723403	-0.089365
27	1	0	1.267522	0.197980	2.735023
28	1	0	0.605931	-0.266681	5.050201
29	1	0	1.895688	0.695434	6.956899
30	1	0	3.892977	2.093474	6.507692
31	1	0	5.399042	3.166343	4.947739
32	1	0	-1.513806	1.422320	-1.454119
33	1	0	-2.474022	3.076399	0.123590
34	1	0	-1.064569	3.982047	1.972664
35	1	0	1.240882	3.211079	2.277223
36	1	0	0.336840	0.060929	-2.199354
37	14	0	2.986700	-1.163909	-2.672192
38	14	0	6.913924	4.041184	2.563871
39	6	0	1.503164	-2.003224	-3.508494
40	1	0	0.868700	-1.295240	-4.054758
41	1	0	1.865025	-2.739097	-4.237745
42	1	0	0.871117	-2.537712	-2.789469
43	6	0	3.946159	-0.198031	-3.985700
44	1	0	4.722945	0.430145	-3.538060
45	1	0	4.413851	-0.881347	-4.707025
46	1	0	3.272440	0.460823	-4.547227
47	6	0	4.052619	-2.518602	-1.891221
48	1	0	4.976117	-2.121524	-1.460974
49	1	0	3.508995	-3.032991	-1.089597
50	1	0	4.320845	-3.272191	-2.642997
51	6	0	8.479456	3.003881	2.328993
52	1	0	8.481646	2.448232	1.387220
53	1	0	9.361592	3.657673	2.337640
54	1	0	8.593402	2.280805	3.145591
55	6	0	6.673365	5.232413	1.114408
56	1	0	6.569984	4.701677	0.163703
57	1	0	5.774475	5.845626	1.251139
58	1	0	7.530139	5.914117	1.038560
59	6	0	7.137165	5.069169	4.144363
60	1	0	7.369193	4.452575	5.020934
61	1	0	7.975136	5.764767	4.010193
62	1	0	6.248405	5.666693	4.378963
63	6	0	9.774642	3.268171	-4.474388
64	6	0	11.117829	3.578979	-4.538191
65	6	0	12.041729	3.108256	-3.584213
66	6	0	11.645762	2.236729	-2.587025

67	6	0	10.231410	1.861605	-2.469615
68	6	0	9.303359	2.435923	-3.443292
69	8	0	7.996296	2.293117	-3.371644
70	6	0	12.548153	1.709527	-1.573736
71	6	0	12.213996	0.705816	-0.749744
72	6	0	11.265270	-1.402171	-1.611190
73	6	0	10.142252	-1.658379	-2.525086
74	6	0	9.232712	-0.592374	-2.504493
75	6	0	9.768139	0.585673	-1.678193
76	6	0	9.907638	-2.838300	-3.235526
77	6	0	8.711286	-2.956841	-3.935259
78	6	0	7.769976	-1.918536	-3.883922
79	6	0	8.011123	-0.740468	-3.171086
80	8	0	8.813518	1.269930	-0.872315
81	8	0	12.236659	-2.104264	-1.410205
82	53	0	14.514402	2.575517	-1.340492
83	1	0	9.052776	3.671503	-5.175843
84	1	0	11.473387	4.234754	-5.328544
85	1	0	13.075277	3.425767	-3.646362
86	1	0	9.654389	2.323036	-1.429415
87	1	0	7.651285	1.911074	-2.518433
88	1	0	12.920329	0.351236	-0.006344
89	1	0	10.644284	-3.635797	-3.210528
90	1	0	8.492568	-3.858562	-4.500267
91	1	0	6.821776	-2.030622	-4.402430
92	1	0	7.240542	0.016711	-3.133793
93	6	0	10.941617	-0.076296	-0.854536
94	6	0	10.445926	-0.476063	0.555928
95	1	0	11.225038	-1.057103	1.059654
96	1	0	10.212508	0.413087	1.145933
97	1	0	9.542305	-1.089634	0.494915

Optimized Cartesian coordinates for **r-tsi12-0**

Center Number	Atomic Number	Atomic Type	Coordinates (Angstroms)		
			X	Y	Z

1	15	0	2.066680	2.475600	-1.784545
2	8	0	2.547961	1.192125	-0.890970
3	8	0	0.478730	2.185963	-2.031144
4	8	0	2.292740	3.692588	-0.913463
5	8	0	2.686085	2.491685	-3.171059
6	6	0	1.371339	-2.674556	-1.958006
7	6	0	0.383735	-1.739714	-1.511256
8	6	0	-0.982469	-2.131858	-1.573270
9	6	0	-1.343910	-3.383104	-2.023851
10	6	0	-0.362155	-4.316646	-2.431864
11	6	0	0.967152	-3.963138	-2.400222
12	6	0	2.738302	-2.292852	-1.956410
13	6	0	3.159633	-1.019303	-1.618463
14	6	0	2.144821	-0.102643	-1.219697
15	6	0	0.808970	-0.440474	-1.059231
16	6	0	-0.927541	0.154828	0.717116
17	6	0	-1.944395	1.049988	1.179699
18	6	0	-2.718345	0.702118	2.319667
19	6	0	-2.485561	-0.468908	3.003462
20	6	0	-1.456838	-1.338683	2.571080
21	6	0	-0.701065	-1.038114	1.458518
22	6	0	-0.158250	0.515856	-0.445050
23	6	0	-0.338666	1.785329	-0.972453
24	6	0	-1.361489	2.686988	-0.561372
25	6	0	-2.153969	2.275473	0.495007
26	1	0	3.835694	3.400366	-3.336683
27	1	0	-1.749388	-1.426451	-1.275480
28	1	0	-2.395531	-3.653257	-2.070988
29	1	0	-0.660965	-5.302110	-2.778620

Copy rights @ Nan Lu,

30	1	0	1.733643	-4.662604	-2.726229
31	1	0	3.465882	-3.044396	-2.252935
32	1	0	-3.492977	1.390823	2.649310
33	1	0	-3.078187	-0.721844	3.878405
34	1	0	-1.256141	-2.251631	3.125472
35	1	0	0.090245	-1.711358	1.150080
36	1	0	-2.964477	2.910512	0.844457
37	14	0	-1.692739	4.368929	-1.397154
38	14	0	5.018735	-0.596499	-1.658720
39	6	0	-3.470391	4.882497	-0.969679
40	1	0	-3.611730	5.057969	0.103341
41	1	0	-3.714688	5.820896	-1.483562
42	1	0	-4.204613	4.132838	-1.287701
43	6	0	-0.511781	5.682673	-0.716928
44	1	0	-0.737966	5.896423	0.334952
45	1	0	0.526999	5.342597	-0.767624
46	1	0	-0.607241	6.622237	-1.276517
47	6	0	-1.560764	4.244923	-3.281141
48	1	0	-2.224983	3.464480	-3.671659
49	1	0	-1.854969	5.194426	-3.746137
50	1	0	-0.545025	4.001530	-3.605176
51	6	0	5.465281	0.282747	-3.273304
52	1	0	4.863253	1.183878	-3.417450
53	1	0	6.525006	0.567867	-3.279672
54	1	0	5.289943	-0.375496	-4.132982
55	6	0	5.531639	0.434026	-0.157100
56	1	0	5.066136	1.423229	-0.157883
57	1	0	5.246977	-0.063280	0.778041
58	1	0	6.621400	0.564436	-0.144365
59	6	0	5.977298	-2.234885	-1.589797
60	1	0	5.802570	-2.866605	-2.468865
61	1	0	7.054329	-2.027549	-1.552418
62	1	0	5.724778	-2.821731	-0.698684
63	6	0	4.266760	7.750824	-1.442957
64	6	0	3.968978	8.776751	-2.315562
65	6	0	3.234126	8.566936	-3.510409
66	6	0	2.822515	7.295510	-3.834305
67	6	0	3.173846	6.169958	-2.992353
68	6	0	3.805748	6.440954	-1.719400
69	8	0	4.000671	5.512844	-0.824611
70	53	0	0.518058	8.108434	-5.777531
71	6	0	2.161993	6.913503	-5.082330
72	6	0	2.568712	5.849872	-5.784971
73	6	0	3.839367	5.059890	-5.510195
74	6	0	4.478828	5.146626	-4.073811
75	6	0	4.911969	5.769019	-6.410667
76	6	0	5.963810	6.322013	-5.535072
77	6	0	5.737558	5.953055	-4.206618
78	6	0	7.119426	7.009166	-5.918493
79	6	0	8.053270	7.320224	-4.934505
80	6	0	7.843368	6.922260	-3.602504
81	6	0	6.692885	6.228379	-3.226535
82	8	0	4.862409	5.819151	-7.622152
83	1	0	4.781652	7.928676	-0.504930
84	1	0	4.293737	9.785862	-2.075200
85	1	0	3.005397	9.404286	-4.160644
86	1	0	3.380408	4.681148	-0.936039
87	1	0	2.077111	5.581810	-6.714641
88	1	0	7.274202	7.268946	-6.961224
89	1	0	8.961319	7.856003	-5.196107
90	1	0	8.597125	7.150296	-2.853942
91	1	0	6.549470	5.899134	-2.203030
92	6	0	3.668834	3.601206	-5.980935
93	1	0	2.874596	3.095434	-5.427947
94	1	0	3.429308	3.607337	-7.048224
95	1	0	4.595983	3.037943	-5.840556

| 96 | 8 | 0 | 4.656148 | 4.047040 | -3.359923 |
| 97 | 1 | 0 | 2.472640 | 5.339504 | -2.994586 |

Optimized Cartesian coordinates for **r-tsi12-1**

Center Number	Atomic Number	Atomic Type	Coordinates (Angstroms) X	Y	Z
1	15	0	1.688512	2.536840	-1.895540
2	8	0	2.485943	1.342194	-1.134196
3	8	0	0.136497	2.049714	-1.868752
4	8	0	1.973080	3.838210	-1.229841
5	8	0	2.028775	2.449775	-3.426092
6	6	0	1.593324	-2.658120	-1.970025
7	6	0	0.599919	-1.835295	-1.350316
8	6	0	-0.701330	-2.380090	-1.168677
9	6	0	-0.991630	-3.670848	-1.554784
10	6	0	0.002006	-4.492309	-2.137331
11	6	0	1.266816	-3.990405	-2.341065
12	6	0	2.888848	-2.126103	-2.201067
13	6	0	3.215759	-0.808423	-1.934837
14	6	0	2.182784	-0.005376	-1.372774
15	6	0	0.945548	-0.488088	-0.976604
16	6	0	-0.490253	-0.067872	1.093457
17	6	0	-1.496367	0.717106	1.741899
18	6	0	-1.998543	0.305220	3.006007
19	6	0	-1.512165	-0.821375	3.628241
20	6	0	-0.492811	-1.579983	3.005975
21	6	0	0.002908	-1.216335	1.772584
22	6	0	0.001093	0.358513	-0.190762
23	6	0	-0.423508	1.586333	-0.671483
24	6	0	-1.446118	2.376537	-0.075721
25	6	0	-1.969261	1.898279	1.112683
26	1	0	2.229513	3.404867	-3.806892
27	1	0	-1.478034	-1.761618	-0.734356
28	1	0	-1.996713	-4.059582	-1.414726
29	1	0	-0.239237	-5.510110	-2.431273
30	1	0	2.037757	-4.603596	-2.802037
31	1	0	3.636138	-2.796589	-2.617713
32	1	0	-2.770155	0.908834	3.478376
33	1	0	-1.898162	-1.123653	4.597873
34	1	0	-0.092167	-2.456472	3.508183
35	1	0	0.791459	-1.803412	1.316581
36	1	0	-2.765584	2.444484	1.611980
37	14	0	-2.135055	3.987292	-0.833855
38	14	0	4.997765	-0.192336	-2.220761
39	6	0	-3.828083	4.308456	-0.035226
40	1	0	-3.756107	4.506600	1.040832
41	1	0	-4.287100	5.193063	-0.494599
42	1	0	-4.519046	3.469088	-0.177445
43	6	0	-1.002532	5.448655	-0.440501
44	1	0	-0.964723	5.627276	0.641110
45	1	0	0.022458	5.274175	-0.780617
46	1	0	-1.378673	6.364234	-0.915518
47	6	0	-2.394314	3.807267	-2.699654
48	1	0	-3.037344	2.949112	-2.929496
49	1	0	-2.883791	4.703915	-3.101043
50	1	0	-1.450200	3.664267	-3.232795
51	6	0	5.114828	0.918739	-3.745651
52	1	0	4.443685	1.777530	-3.663881
53	1	0	6.139368	1.289574	-3.874161
54	1	0	4.839452	0.365847	-4.651829
55	6	0	5.629927	0.707174	-0.679642
56	1	0	5.031127	1.596373	-0.462365
57	1	0	5.593640	0.055493	0.201701
58	1	0	6.672764	1.019027	-0.819382

59	6	0	6.091440	-1.716180	-2.511167
60	1	0	5.819227	-2.260795	-3.423165
61	1	0	7.136052	-1.399898	-2.624889
62	1	0	6.052337	-2.421353	-1.672574
63	6	0	2.511897	8.690544	-2.470548
64	6	0	2.619425	9.668928	-3.438335
65	6	0	2.852120	9.360998	-4.793702
66	6	0	3.062347	8.055710	-5.197537
67	6	0	2.961602	6.969846	-4.217063
68	6	0	2.661329	7.341054	-2.834804
69	8	0	2.423812	6.450634	-1.894220
70	53	0	3.047347	9.118759	-8.156882
71	6	0	3.310796	7.667262	-6.577640
72	6	0	3.683872	6.428820	-6.932294
73	6	0	4.022083	5.333782	-5.966643
74	6	0	3.577269	5.547425	-4.465100
75	6	0	5.578606	5.240020	-5.920345
76	6	0	5.963436	5.096023	-4.509448
77	6	0	4.841472	5.176244	-3.673593
78	6	0	7.244135	4.803025	-4.033249
79	6	0	7.401198	4.570487	-2.671185
80	6	0	6.281027	4.602820	-1.827476
81	6	0	5.001959	4.894878	-2.310210
82	8	0	6.306129	5.228858	-6.893970
83	1	0	2.284586	8.920577	-1.435586
84	1	0	2.490581	10.710471	-3.156033
85	1	0	2.878092	10.161884	-5.521954
86	1	0	2.335804	5.518272	-2.237534
87	1	0	3.850316	6.187397	-7.977159
88	1	0	8.075500	4.747786	-4.729732
89	1	0	8.381392	4.343015	-2.261649
90	1	0	6.403320	4.385036	-0.769985
91	1	0	4.168225	4.868763	-1.621796
92	6	0	3.504721	3.977164	-6.501197
93	1	0	2.413447	3.975771	-6.548025
94	1	0	3.917460	3.803403	-7.499887
95	1	0	3.817739	3.154383	-5.851986
96	8	0	2.390604	4.836572	-4.113442
97	1	0	1.947913	6.207130	-4.365577

Optimized Cartesian coordinates for **ts-i34**

Center Number	Atomic Number	Atomic Type	Coordinates (Angstroms) X	Y	Z

1	6	0	5.281698	-4.007255	-3.549855
2	6	0	5.639543	-2.704431	-3.849212
3	6	0	6.703935	-2.085033	-3.187181
4	6	0	7.441268	-2.763123	-2.218715
5	6	0	7.109228	-4.132376	-1.913701
6	6	0	5.998194	-4.722085	-2.580694
7	8	0	5.553387	-5.961414	-2.310444
8	6	0	8.592465	-2.152571	-1.542854
9	6	0	9.258311	-2.762503	-0.559003
10	6	0	10.151310	-4.989196	0.091003
11	6	0	9.985116	-6.148302	-0.802465
12	6	0	8.735395	-6.097889	-1.449864
13	6	0	7.995322	-4.889856	-1.028166
14	6	0	10.909923	-7.158387	-1.050870
15	6	0	10.571083	-8.142096	-1.977303
16	6	0	9.331792	-8.100600	-2.637654
17	6	0	8.407125	-7.088485	-2.389692
18	8	0	6.608012	-5.846174	0.132578
19	8	0	11.105902	-4.707280	0.781675
20	53	0	9.273963	-0.187078	-2.105259
21	1	0	4.440637	-4.499959	-4.025299

22	1	0	5.081969	-2.149387	-4.597968
23	1	0	6.966497	-1.065403	-3.438130
24	1	0	6.052502	-5.150810	0.528204
25	1	0	5.868491	-6.233029	-1.414403
26	1	0	10.086664	-2.295757	-0.037053
27	1	0	11.862289	-7.159214	-0.530509
28	1	0	11.266646	-8.947453	-2.193930
29	1	0	9.081688	-8.879598	-3.351337
30	1	0	7.449176	-7.094763	-2.893922
31	6	0	8.866959	-4.121060	-0.027298
32	6	0	8.284375	-3.891719	1.394472
33	1	0	9.015829	-3.315217	1.966938
34	1	0	7.354581	-3.316761	1.344117
35	1	0	8.118498	-4.837289	1.911129
36	13	0	6.499857	-7.383083	1.188619
37	17	0	4.972150	-6.780688	2.574468
38	17	0	8.413929	-7.714910	2.093634
39	17	0	5.926220	-8.927550	-0.180993

Optimized Cartesian coordinates for **ts-i56-0**

Center Number	Atomic Number	Atomic Type	Coordinates (Angstroms) X	Y	Z

1	6	0	4.396947	-5.808628	-3.918407
2	6	0	4.568848	-4.542621	-4.426827
3	6	0	5.435180	-3.607104	-3.817267
4	6	0	6.160594	-3.945590	-2.687343
5	6	0	6.041478	-5.281950	-2.161861
6	6	0	5.094377	-6.211844	-2.740695
7	8	0	4.843265	-7.335773	-2.162903
8	6	0	7.112224	-3.038128	-2.035592
9	6	0	7.771130	-3.351889	-0.914260
10	6	0	8.897049	-5.284384	0.152685
11	6	0	9.024201	-6.571497	-0.478993
12	6	0	7.828224	-6.864743	-1.179452
13	6	0	6.876622	-5.719025	-1.076063
14	6	0	10.116614	-7.454668	-0.465235
15	6	0	9.996698	-8.647100	-1.165736
16	6	0	8.811450	-8.945140	-1.860433
17	6	0	7.722956	-8.071768	-1.875900
18	8	0	5.619930	-6.708497	0.095438
19	8	0	9.699326	-4.677596	0.891898
20	53	0	7.487292	-1.086876	-2.865308
21	1	0	3.711194	-6.521562	-4.364359
22	1	0	4.021524	-4.241034	-5.316234
23	1	0	5.546510	-2.623498	-4.255622
24	1	0	4.937912	-6.074698	0.384428
25	1	0	5.217226	-7.147182	-0.800809
26	1	0	8.450447	-2.661821	-0.425799
27	1	0	11.028076	-7.205546	0.064685
28	1	0	10.821438	-9.352515	-1.177075
29	1	0	8.735407	-9.886550	-2.397337
30	1	0	6.805728	-8.331513	-2.389574
31	6	0	7.543213	-4.662439	-0.182048
32	6	0	6.794123	-4.342144	1.141806
33	1	0	7.364511	-3.594793	1.699205
34	1	0	5.809340	-3.922556	0.914913
35	1	0	6.684136	-5.235672	1.760793
36	13	0	11.358166	-4.715921	1.800477
37	17	0	11.364515	-2.848991	2.813719
38	17	0	12.789123	-4.917247	0.224374
39	17	0	11.182024	-6.446733	3.042444

Optimized Cartesian coordinates for **ts-i56-1**

Center Number	Atomic Number	Atomic Type	X	Y	Z
			Coordinates (Angstroms)		
1	6	0	-3.228950	3.258421	-1.528275
2	6	0	-4.220582	2.286502	-1.566383
3	6	0	-3.982835	0.963604	-1.160434
4	6	0	-2.716167	0.576160	-0.728552
5	6	0	-1.701354	1.587631	-0.686764
6	6	0	-1.950737	2.910615	-1.067532
7	8	0	-0.986534	3.860597	-1.042033
8	6	0	-2.353870	-0.777296	-0.226019
9	6	0	-1.081771	-1.188951	-0.061689
10	6	0	1.392784	-0.055884	0.142354
11	6	0	1.108815	0.563003	1.477632
12	6	0	-0.045377	1.344819	1.270917
13	6	0	-0.469335	1.113719	-0.101504
14	6	0	1.759883	0.533436	2.695826
15	6	0	1.210552	1.311930	3.726906
16	6	0	0.064457	2.098710	3.529098
17	6	0	-0.578031	2.137165	2.289908
18	8	0	1.464971	1.556550	-0.610798
19	8	0	2.383394	-0.826852	-0.118440
20	53	0	-3.929652	-2.157330	0.255875
21	1	0	-3.415202	4.279000	-1.844677
22	1	0	-5.212618	2.557060	-1.915711
23	1	0	-4.794129	0.245212	-1.172047
24	1	0	1.887464	1.453143	-1.494207
25	1	0	-0.119740	3.463360	-0.834456
26	1	0	-0.826957	-2.192001	0.263383
27	1	0	2.665758	-0.045790	2.838828
28	1	0	1.689000	1.313108	4.702057
29	1	0	-0.325658	2.687084	4.353956
30	1	0	-1.466519	2.741290	2.133704
31	6	0	0.010140	-0.242144	-0.555935
32	6	0	0.169058	-0.523290	-2.064672
33	1	0	0.420285	-1.580263	-2.193623
34	1	0	-0.766044	-0.328636	-2.595182
35	1	0	0.968045	0.056165	-2.529071
36	13	0	4.134425	-0.642228	-0.591082
37	17	0	4.826661	-2.619503	-0.984711
38	17	0	5.157186	0.351621	1.012831
39	17	0	4.003672	0.595097	-2.379460

Optimized Cartesian coordinates for **ts-i56-2**

Center Number	Atomic Number	Atomic Type	X	Y	Z
			Coordinates (Angstroms)		
1	6	0	1.177339	4.225721	-1.627464
2	6	0	2.321823	3.452102	-1.846228
3	6	0	2.547196	2.284713	-1.129910
4	6	0	1.597873	1.798182	-0.218400
5	6	0	0.322987	2.492933	-0.108511
6	6	0	0.214262	3.773205	-0.743705
7	8	0	-0.793947	4.637185	-0.447655
8	6	0	1.833371	0.638902	0.615468
9	6	0	0.906809	0.212101	1.502138
10	6	0	-1.621159	-0.461417	0.925027
11	6	0	-2.702704	0.545818	0.601221
12	6	0	-2.182658	1.822507	0.263439
13	6	0	-0.746527	1.826552	0.554454
14	6	0	-4.054181	0.241498	0.505310
15	6	0	-4.913348	1.201519	-0.027500
16	6	0	-4.413782	2.444446	-0.444235
17	6	0	-3.067838	2.763830	-0.311404
18	8	0	-1.987853	-1.289875	1.951268

19	8	0	-1.063735	-1.028140	-0.143129
20	53	0	3.719478	-0.381757	0.575038
21	1	0	1.045859	5.196285	-2.093218
22	1	0	3.074906	3.801883	-2.546054
23	1	0	3.474309	1.743061	-1.265391
24	1	0	-1.566554	-2.170365	1.818997
25	1	0	-1.222594	4.371627	0.381520
26	1	0	1.128253	-0.583551	2.206135
27	1	0	-4.407928	-0.746143	0.778991
28	1	0	-5.966929	0.971975	-0.157381
29	1	0	-5.088260	3.175431	-0.880096
30	1	0	-2.731991	3.729637	-0.661104
31	6	0	-0.443765	0.759056	1.522436
32	6	0	-0.912155	1.073034	2.966325
33	1	0	-0.818518	0.169281	3.572521
34	1	0	-0.292342	1.863465	3.402859
35	1	0	-1.957207	1.389916	2.985912
36	13	0	-1.222376	-2.652385	-0.902353
37	17	0	0.234525	-2.755604	-2.460264
38	17	0	-3.254334	-2.903212	-1.570347
39	17	0	-0.793584	-4.017818	0.759561